An analytical study on M₂ tidal wave in the Taiwan Strait with the extended Taylor's method

Di Wu[1], Guohong Fang[1,2], Xinmei Cui[1,2], Fei Teng[1,2]

[1]The First Institute of Oceanography, State Oceanic Administration, Qingdao, 266061, China

5 [2]Laboratory for Regional Oceanography and Numerical Modeling, Qingdao National Laboratory for Marine Science and Technology, Qingdao, 266237, China

Correspondence to: Guohong Fang (fanggh@fio.org.cn)

Abstract. The tides in the Taiwan Strait (TS) are featured by large M₂ amplitudes. The extended Taylor's method is employed in this study to provide an analytical model for the M₂ tide in the TS. The strait is idealized as a rectangular basin

10 with a uniform depth, but the Coriolis and friction forces are retained in the governing equations. The observed tides at the northern and southern openings are used as open boundary conditions. The obtained analytical solution, which consists of a stronger southward propagating Kelvin wave, a weaker northward propagating Kelvin wave, and two families of Poincaré modes trapped at the northern and southern openings, agrees well with the observations in the strait. The superposition of two Kelvin waves can basically represent the observed tidal pattern, including an anti-nodal band in the central strait, and the

15 cross-strait asymmetry (greater amplitudes in the west and smaller in the east) of the anti-nodal band. The superposition of Poincaré modes can further improve the model result in that the cross-strait asymmetry can be better reproduced. In order to explore the formation mechanism of the northward propagating wave in the TS three experiments are carried out, including the deep basin south of the strait. The results show that the southward incident wave can be reflected to form a northward wave by the abruptly deepened topography south of the strait, but the reflected wave is slightly weaker than the northward

20 wave obtained from above analytical solution, in which the southern open boundary condition is specified with observations. The forcing at the Luzon Strait can strengthen the northward Kelvin wave in the TS, and thus is of secondary importance to the M₂ tide in the TS.

1 Introduction

The Taiwan Strait (TS) is the sole passage connecting the East China Sea (ECS) and South China Sea (SCS).The strait is

25 about 350 km long, 200 km wide and mostly located on the continental shelf with a mean depth of about 50 metres. The bottom topography of the TS can be viewed as the extension of the ECS shelf in the north and becomes irregular in the south. The SCS deep basin is located south of the strait and is connected to the Pacific Ocean through the Luzon Strait (LS). An abrupt depth change is present between the TS and the SCS deep basin (Fig. 1).

The tides in the strait feature large M₂ amplitudes. The greatest amplitude by tidal gauge observation along the western

Taiwan coast reported by Jan et al. (2004b) is 1.73 m at Taichung, while that along the mainland coast is 2.10 m at Matsu. Matsu is an island located about 20 km away from the coast, the satellite observation indicates that the greatest amplitude, exceeding 2.2 m, appears near Haitan Island, which is located south of Matsu (Fig. 2). Thus the tidal regime of the M_2 constituent has an anti-nodal band near the cross-strait line from Haitan to Taichung, with greater amplitudes in the west and

5 smaller in the east, which is called the asymmetry by Yu et al. (2015). The tides in the TS have attracted a great number of studies since 1980s (Yin and Chen, 1982; Fang et al., 1984; Ye et al., 1985; Lü et al., 1999; Lin et al., 2000; Lin et al., 2001; Jan et al., 2002; Jan et al., 2004a; Jan et al., 2004b; Zhu, et al., 2009; Hu et al., 2010; Zeng et al., 2012; Yu et al., 2015; Yu et al., 2017). Most investigators have recognized that the semidiurnal tides in the TS mainly consist of two oppositely propagating waves, one from north to south and another from the south to north. In particular, Fang et al. (1984, 1999)

10 suggested that the semidiurnal tidal motion in the TS was maintained mainly by the energy flux from the ECS and partly by that from the SCS. Jan et al. (2002, 2004) further noticed that the southward propagating wave could be reflected when encountering the sharply deepened bottom topography south of the strait, and suggested that the reflected wave was the main component of the northward propagating wave, and the contribution of the SCS was negligible. Yu et al. (2015) made an extensive numerical study on the formation of the M_2 tide in the strait with special focus on the asymmetric nature in the

15 cross-strait direction.

The existing studies almost all employed data analysis and numerical modeling, except that some simple dynamical analyses were performed using one-dimensional solutions to explain the model results in Jan et al. (2002) and Yu et al. (2015). The purpose of the present study is to establish two-dimensional analytical models using the extended Taylor's method. In the analytical models the classical Kelvin waves and Poincaré modes in idealized basins are used to

20 approximately represent the tides in the natural basin, and thus enable us to estimate the strengths of the southward and the northward waves, to reveal the role of each classical wave in the formation of the tides in the strait, and to clarify how the waves are generated. In particular, we can roughly estimate the relative importance of the reflected wave at steep topography versus the incident wave from the LS in the formation of the northward Kelvin wave in the TS.

Taylor's problem is a classical tidal dynamic problem. Since his pioneering work Taylor's method has been subsequently

25 developed and applied to many sea areas (e. g., Roos and Velema, 2011, Table 1). In the previous applications all the studied basins have a closed end that can almost perfectly reflect the incident tidal wave closely retaining the phase of the tidal elevation. In contrast, the topographic step south of the TS acts as a permeable interface which can only partially reflect the incident wave, and furthermore, the elevation phase of the reflected wave is changed by nearly 180 ° at the step. Therefore, the strait is also a locality of particular interest for the application of the Taylor's method.
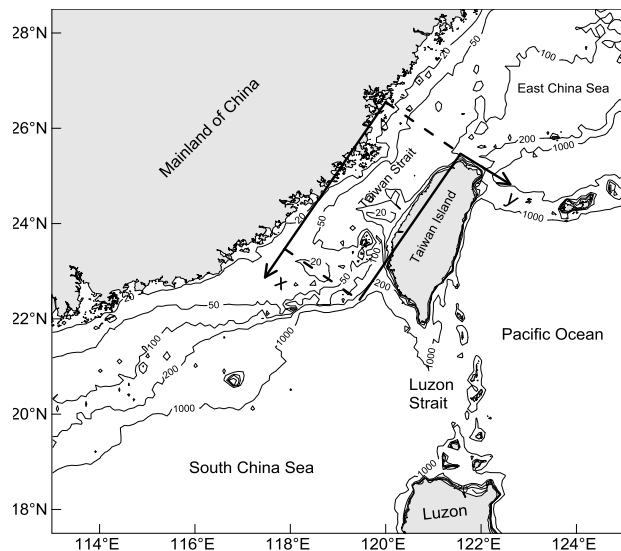
Figure 1. Bathymetric chart of the Taiwan Strait and its neighbouring area, the rectangle indicates the idealized model basin representing the Taiwan Strait. Isobaths are in metres (based on ETOPO1 from the US National Geophysical Center).
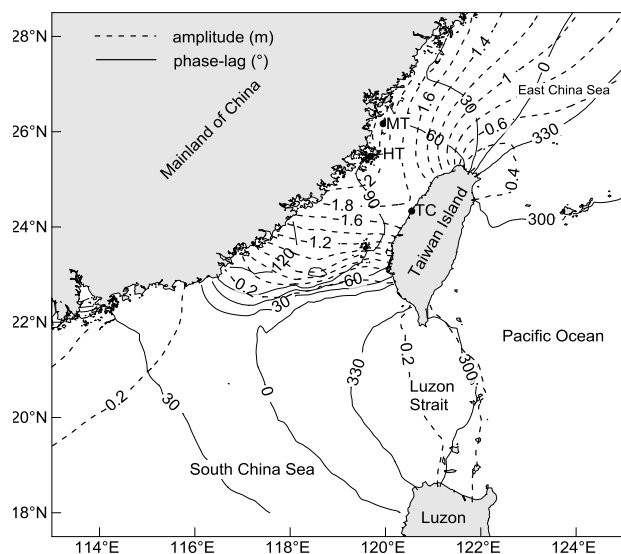
5   **Figure 2.** Cotidal chart of M_2 constituent in the Taiwan Strait (based on DTU10, see Chen and Andersen, 2011). (MT-Matsu, HT-Haitan, TC-Taichung)

2 Solution Method

Taylor (1922) first presented an analytical solution for tides in a semi-infinite rotating channel of uniform depth to explain the existence of amphidromic systems in gulfs. His solution showed that the tide in such a channel can be represented by the

10   superposition of an incident Kelvin wave, a reflected Kelvin wave and a family of Poincaré modes trapped near the closed end. Defant in 1925 simplified Taylor's solution approach by introducing the collocation method (see Defant, 1961, pp.213-

215). In the original Taylor's problem as well as the Defant' approach the friction and open boundary condition were left out

of consideration. Fang and Wang (1966) and Rienecker and Teubner (1980) extended the Taylor's problem by taking friction

into consideration. The introduction of friction can explain why the amphidromic point in the northern hemisphere shifts

from the central axis towards the right as seen from the closed end and looking seawards. Fang et al. (1991) further extended

5   the Taylor's problem by introducing the open boundary condition, enabling solutions for open rectangular basins. Jung et al.

(2005) and Roos and Velema (2011) further extended the Taylor's method to model tides with multiple rectangular basins.

Solution method used in the present study is basically the same as Fang et al. (1991), but with minor correction and

generalization as done in studies of Jung et al. (2005) and Roos and Velema (2011). The analytical method initiated by Taylor

and developed afterward is called the extended Taylor's method in this paper.

10   **2.1 Governing equations and boundary conditions**

The governing equations used in this study are as follows:

$$
\begin{cases}
\frac{\partial \tilde{u}}{\partial t} - f\tilde{v} = -g\frac{\partial \tilde{\zeta}}{\partial t} - \gamma\tilde{u} \\
\frac{\partial \tilde{v}}{\partial t} + f\tilde{u} = -g\frac{\partial \tilde{\zeta}}{\partial t} - \gamma\tilde{v} \\
\frac{\partial \tilde{\zeta}}{\partial t} = -h\left[\frac{\partial \tilde{u}}{\partial x} + \frac{\partial \tilde{v}}{\partial y}\right]
\end{cases}
\tag{1}
$$

where t represents time; (x, y) the Cartesian coordinates; $(\tilde{u}, \tilde{v})$ the velocity components in (x, y) directions; $\tilde{\zeta}$ the tidal

elevation; h the water depth, assumed uniform; γ the frictional coefficient, taken constant; $g = 9.8 \text{ ms}^{-2}$ is the

15   acceleration due to gravity; f is the Coriolis parameter, also taken as a constant due to smallness of the study area. When

one cosine wave is considered, $(\tilde{\zeta}, \tilde{u}, \tilde{v})$ can be expressed as

$$
(\tilde{\zeta}, \tilde{u}, \tilde{v}) = \text{Re}(\zeta, u, v)e^{i\sigma t}
\tag{2}
$$

where σ is the angular frequency of the wave, $\text{i} \equiv \sqrt{-1}$. For this wave Eqs. (1) reduce to

$$
\begin{cases}
(\mu + \text{i})u - \nu v = -\frac{g}{\sigma}\frac{\partial \zeta}{\partial x} \\
(\mu + \text{i})u + \nu u = -\frac{g}{\sigma}\frac{\partial \zeta}{\partial y} \\
\zeta = \frac{\text{i}h}{\sigma}\left[\frac{\partial u}{\partial x} + \frac{\partial v}{\partial y}\right]
\end{cases}
\tag{3}
$$

20   in which $\mu = \frac{\gamma}{\sigma}$, $\nu = \frac{f}{\sigma}$.

Consider a rectangular basin with two parallel sidewalls of length L and with a width of B, we put the x axis along a

sidewall and the y axis perpendicular to the x axis and pointing to another sidewall. Thus the basin is confined by $x =$

$0, L$ and $y = 0, B$, respectively. The boundary conditions along the sidewalls are taken

$v = 0$ at $y = 0$ and $y = B$ $\tag{4}$

25   within $x \in (0, L)$. Along the cross sections $x = 0$ and $x = L$, various choices of boundary conditions are applicable

depending on the problem concerned:

$u = 0$, if the cross section is a closed boundary $\tag{5}$

$u = \pm\sqrt{\frac{g}{h}}\,\zeta$, if the free radiation in the positive/negative x direction occurs on the cross section ⟶ (6)

$\zeta = \hat{\zeta}$, if the tidal elevation is specified as $\hat{\zeta}$ along the cross section ⟶ (7)

and/or,

$\zeta_A = \zeta_B$ and $u_A h_A = u_B h_B$, if the cross section is a connecting boundary of two basins A and B. ⟶ (8)

5 Eqs. (8) are matching conditions accounting for sea level continuity and volume transport continuity respectively. The individual equations (5) to (8) or their combination may be used as boundary conditions on the cross sections. Strictly speaking, Eq. (6) is valid only in the frictionless case, if friction is considered it contains an error of the order of μ^2, and there is a phase difference between u and ζ (Fang and Wang, 1966). In the present study we still use the form of Eq. (6) due to smallness of the value of μ.

10 **2.2 General solution and collocation method**

The governing equations (3) have only the following four forms satisfying the sidewall boundary condition (4) (see Fang et al., 1991, an error in the equation for β in their paper has been corrected here):

$$\begin{cases} v_1 = 0 \\ u_1 = -a\exp(\alpha y + i\beta x) \\ \zeta_1 = \frac{\beta}{\sigma}ha\exp(\alpha y + i\beta x) \end{cases}$$ ⟶ (9)

$$\begin{cases} v_2 = 0 \\ u_2 = b\,\exp[-(\alpha y + i\beta x)] \\ \zeta_2 = \frac{\beta}{\sigma}hb\,\exp[-(\alpha y + i\beta x)] \end{cases}$$ ⟶ (10)

15 $$\begin{cases} v_3 = \sum_{n=1}^{\infty}\kappa_n\sin r_n y\exp(-s_n x) \\ u_3 = \sum_{n=1}^{\infty}\kappa_n(A_n\cos r_n y + B_n\sin r_n y)\exp(-s_n x) \\ \zeta_3 = \frac{ih}{\sigma}\sum_{n=1}^{\infty}\kappa_n(C_n\cos r_n y + D_{1,n}\sin r_n y)\exp(-s_n x) \end{cases}$$ ⟶ (11)

and

$$\begin{cases} v_4 = \sum_{n=1}^{\infty}\lambda_n\sin r_n y\exp[-s_n(L-x)] \\ u_4 = \sum_{n=1}^{\infty}\lambda_n(A'_n\cos r_n y + B'_n\sin r_n y)\exp[-s_n(L-x)] \\ \zeta_4 = \frac{ih}{\sigma}\sum_{n=1}^{\infty}\lambda_n(C'_n\cos r_n y + D'_n\sin r_n y)\exp[-s_n(L-x)] \end{cases}$$ ⟶ (12)

where

$$\alpha = \frac{\nu}{(1-i\mu)^{\frac{1}{2}}}k$$ ⟶ (13)

20 $$\beta = (1-i\mu)^{\frac{1}{2}}k$$ ⟶ (14)

$$r_n = \frac{n\pi}{B}$$ ⟶ (15)

$$s_n = (r_n^2 - Q^2)^{\frac{1}{2}}$$ ⟶ (16)

in which $k = \sigma/c$ is the wave number of the Kelvin wave in absence of friction and $c = \sqrt{gh}$ is the wave speed. In Eq. (16), $Q^2 = \frac{(1-i\mu)^2 - \nu^2}{1-i\mu}k^2$; s_n has two complex values and here we choose the one that has a positive real part. In order to

25 satisfy Eqs. (3), (A_n, B_n, C_n, D_n) and (A'_n, B'_n, C'_n, D'_n) should be

$$A_n = \frac{[(\mu+i)^2+\nu^2]r_n s_n}{(\mu+i)^2 r_n^2+\nu^2 s_n^2} \tag{17}$$

$$B_n = \frac{\nu(\mu+i)Q^2}{(\mu+i)^2 r_n^2+\nu^2 s_n^2} \tag{18}$$

$$C_n = r_n - s_n A_n \tag{19}$$

$$D_n = -s_n B_n \tag{20}$$

$$A_n' = -A_n \tag{21}$$

$$B_n' = B_n \tag{22}$$

$$C_n' = C_n \tag{23}$$

$$D_n' = -D_n \tag{24}$$

Eqs. (9) and (10) represent Kelvin waves propagating in the $-x$ and x directions respectively; Eqs. (11) and (12) represent

two families of Poincaré modes trapped at the cross sections $x = 0, L$ respectively. $(a, b, \kappa_n, \lambda_n)$ are coefficients related to

amplitudes and phases of Kelvin waves and Poincaré modes. These coefficients are to be determined by boundary

conditions.

The collocation method is convenient in determining the coefficients $(a, b, \kappa_n, \lambda_n)$. The calculation procedure can be as

follows. First, we truncate the family of Poincaré modes, Eqs. (11) and (12), at the N-th order, so that the number of

undetermined coefficients for Poincaré modes is $2N$, the total number of undetermined coefficients (plus those for Kelvin

waves) is thus $2N + 2$. To determine these unknowns we take $N + 1$ equally spaced dots, called collocation points, located

at $y = \frac{B}{2(N+1)}, \frac{3B}{2(N+1)}, \dots, \frac{(2N+1)B}{2(N+1)}$ on both the cross sections $x = 0$ and L. At these points one of the boundary

conditions given by Eqs. (5)-(8) should be satisfied. This yields $2N + 2$ equations. By solving this system of equations we

can obtain $2N + 2$ coefficients $(a, b, \kappa_n, \lambda_n)$. Since the high order Poincaré modes decay from the boundary very fast (e.

g., Godin, 1965), it is generally necessary to retain only a few lower order terms.

3 An analytical model for the Taiwan Strait

3.1 Model configuration and solution

In this section we will first establish an idealized analytical model for the TS. The strait is idealized as a rectangular basin

with two sidewalls roughly along the China mainland and Taiwan coastlines as shown in Fig.1. The width and length of the

model domain are taken as B=200 km and L=330 km respectively. The depth is taken as $h = 52$ m, a mean depth calculated

based on ETOPO1.We put the origin of the coordinates at the northernmost corner of the rectangle, x axis along the

mainland coast, and y axis in offshore direction. The axis of the strait is toward the south by southwest. But for short we

will hereafter simply use "south" to refer "south by southwest", and similarly for other directions. The Coriolis parameter f

is taken $0.594 \times 10^{-4} \text{s}^{-1}$, corresponding to a latitude of $\varphi = 24°\text{N}$. The angular frequency of M₂ tide is $1.4052 \times$

10^{-4}s^{-1}. The friction coefficient γ can be estimated from the relation $\gamma = C_D \left(\frac{8}{3\pi}\right)\frac{U}{h}$, in which C_D and U represent the

drag coefficient and amplitude of the M$_2$ tidal current respectively. If we take C_D equal to 0.0026 and U equal to 0.5 m/s,

then $\mu = \gamma/\sigma$ is approximately equal to 0.15. The families of Poincaré modes are truncated at $N = 19$, and 20 collocation

points are set along both the northern and southern open boundaries. The boundary condition (7) is employed with the values

5   of $\hat{\zeta}$ equal to the observed harmonic constants from the global tide model DTU10 (Cheng and Anderson, 2011).
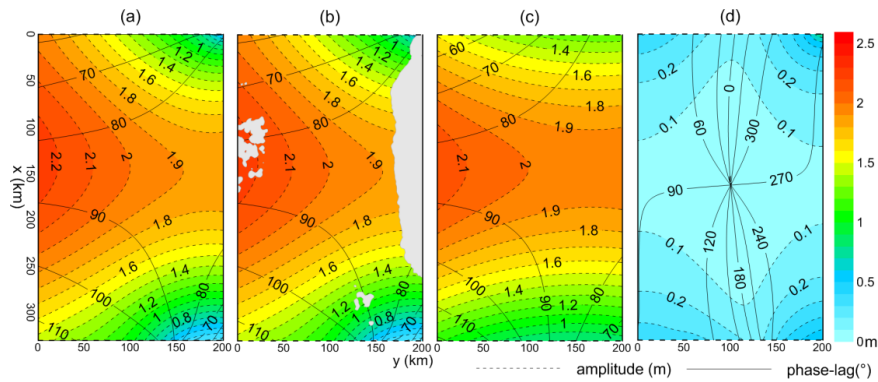
Figure 3. Cotidal charts for M$_2$ constituent: (a) Present analytical model; (b) Observed distribution based on DTU10; (c) Contribution of Kelvin waves; (d) contribution of Poincaré modes. Solid lines represent Greenwich phase-lag; dashed lines represent amplitude (in metres).

10   The obtained analytical solution of M$_2$ constituents is shown in Fig. 3a. For comparison the observed M$_2$ cotidal chart

based on DTU10 is also shown in Fig. 3b. It can be seen that although the complicated bottom topography and the irregular

coastlines are greatly simplified, the analytical model still agrees well with the observation. The observed tidal regime has

the features that the amplitudes are significantly greater along the mainland coast than along the Taiwan coast, showing the

cross-strait asymmetry. The phase-lags near the mainland coast increase from north to south, showing a progressive wave

15   nature, while those near the middle Taiwan coast have only small changes, showing a standing wave nature, that is, the wave

propagates southward in the northeast area and propagates northward in the southeast area. A highest amplitude band is

present roughly along the cross section of $x \approx 150$ km, appearing as an anti-nodal band. The phase-lags in this band range

from 80° to 90°. These features have all been reproduced in the analytical model.

3.2 Kelvin waves and Poincaré modes

20   To reveal the relative importance of the Kelvin waves and Poincaré modes in the model, the superposition of two Kelvin

waves is given in Fig. 3c, and that of Poincaré modes is given in Fig. 3d. It can be observed that the contribution of the

Poincaré modes is much smaller than that of Kelvin waves. The cotidal chart constructed using superposed Kelvin wave

alone (Fig. 3c) resembles the complete model (Fig. 3a) and the observation (Fig. 3b) quite well, though the Poincaré modes

can improve the model to a certain degree. From Fig. 3a we can see that the difference between highest amplitude on the

west sidewall and that on the east sidewall in the anti-nodal band is about 0.4 m; while the corresponding difference shown

in Fig. 3c is about 0.2 m. Thus about a half of the cross-strait asymmetry can be explained by the superposition of two

oppositely propagating Kelvin waves with southward one stronger then the northward one. Here both the Coriolis and

frictional forces are the major factors. The superposition of Poincaré modes in this band has an amplitude of about 0.1 m on

5   both sides, and has a nearly the same phase-lag as the superposed Kelvin wave on the west and a nearly opposite phase-lag

to the superposed Kelvin wave on the east. Therefore, the superposed Poincaré mode plays a role to increase amplitudes in

the west and reduce the amplitudes in the east and hence to enhance the asymmetry. The superposed Poincaré mode has

nearly the same contribution to the cross-strait asymmetry as the superposed Kelvin wave.

From comparison we can find that the amplitude variation along the northern boundary in Fig. 3c is less than that in Fig.

10   3a. This is owing to the fact that the M_2 tide is from the Pacific Ocean, its amplitude increases from the deeper outer shelf

toward the shallower inner shelf. This amplitude variation cannot be completely represented by the superposed Kelvin wave,

and a superposed Poincaré mode is necessary to compensate their difference. The situation at the southern boundary is

similar. The distribution of the superposed Poincaré mode in the anti-nodal band is clearly related to those at the northern and

southern openings (Fig. 3d). Yu et al. (2015) suggested that the orientation of the topographic step south of the strait was not

15   perpendicular to the strait axis, but had an angle. This might cause the reflected wave to propagate toward the mainland coast

and thus amplify the tides there. The present solution indicates that the obliqueness of the topographic step south of the TS

may also play a role in the formation of the cross-strait asymmetry as suggested by Yu et al. (2015), but it is not a controlling

factor.

The obtained analytical solution enables us to see the magnitudes and characteristics of both southward and northward

20   Kelvin waves. These two oppositely propagating waves, which correspond to Eqs. (9) and (10) respectively, are displayed

separately in Figs. 4a and 4b. From Fig. 4a we see that the phase-lag of the southward wave increases from north to south

due to propagation direction. The amplitude deceases from north to south due to friction and from west to east due to

Coriolis effect. The characteristics of the northward wave are opposite. The area mean amplitude of the southward wave is

1.18 m, while that of the northward wave is 0.84 m, smaller than the former by 0.34 m. Along the western sidewall, the

25   amplitudes of the southward wave range from about 1.4 m to 1.6 m, while those of the northward wave range from about 0.6

to 0.7 m, so that the superposition of them is dominated by the former and appears as a southward progressive wave. Around

the cross section $x \approx 150$ km, the phase-lags of the southward and northward waves are nearly equal, between 80 ° and 90 °,

thus the superposed tides have greatest amplitudes, equal to the sum of the amplitudes of these two waves, which exceeds

2.1 m as already seen in Fig. 3c. Along the eastern sidewall, however, the differences of amplitudes of southward and

30   northward waves are much smaller, so that the superposition of them tends to appear as a standing wave. Around the point

$x \approx 150$ km, the phase-lags of the southward and northward waves are also nearly equal, thus the amplitude of combined tide

is also relatively large, equal to the sum of the amplitudes of these two waves, but now it is only slightly greater than 1.9 m,

which is smaller than corresponding value at the western sidewall.
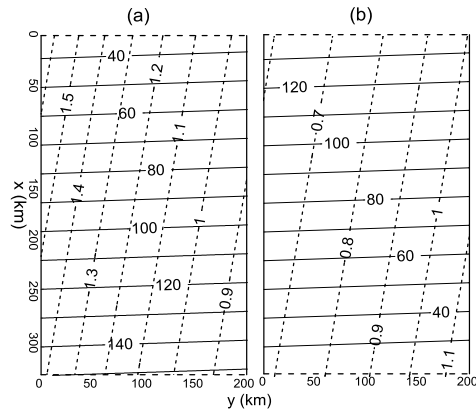
Figure 4. Southward (a) and northward (b) propagating Kelvin waves. Solid lines represent Greenwich phase-lag; dashed lines represent amplitude (in metres).

4 Formation mechanism of the northward Kelvin wave in the Taiwan Strait

There are two possible origins for the northward Kelvin wave in the TS. One is reflection of the southward wave at sharply deepened topography; another is an incident wave from the Luzon Strait propagating toward the TS. In the following we examine their respective contributions by using the extended Taylor's models.

4.1 Reflection of the incident wave from the East China Sea at the topographic step

Three experiments have been carried out to explore the formation mechanism of the northward Kelvin wave in the TS. The first experiment (denoted as Ex. 1) has a model geometry shown in Fig. 5a. The TS is represented by area A, with the width and depth equal to the above single area model. Since the topographic step is located away from the southern boundary of the single area model domain (Fig. 1), we extend the length of the area to 400 km. The area B represents the deep basin south of the topographic step, and the water depth of the deep basin is taken 1000 m as done in Jan et al. (2002 and 2004). The purpose of this experiment is to examine the effect of the topographic step in reflecting the incident wave from the ECS. As in the single basin solution, the open boundary condition (7) is used at the northern opening with values of $\hat{\zeta}$ equal to the observations taken from the global tidal model DTU10. The matching condition (8) is applied at the connecting boundary of areas A and B, and the radiative condition (6) is used at the southernmost opening.

Figure 5b displays the solution of Ex.1. It can be seen that the basic pattern of the tidal regime is similar to that of the single area model solution shown in Fig. 3a. In particular, there is also an anti-nodal band near $x = 150$ km though the amplitudes in this band produced by this experiment are smaller than those given in Fig. 3a. The smallest amplitudes appear along the connecting cross section, showing a nodal band exists there. Therefore, the anti-node is located about 250 km away from the topographic step. The wavelength of M_2 tide in a channel of uniform depth 52 m is equal to 1009 km, so the distance between

the anti-node and the topographic step is equal to one quarter of the wavelength. This result further implies that if the channel were 500 km long, resonance would occur. However, Taiwan Island is about 380 km long, and is not able to support a resonance for M_2 constituent. In fact, the resonant period of the TS is 13.5 h according to the experiments made by Cui et al. (2015), which is almost the same as one of the resonant periods of the ECS (13.7 h), meaning that the tidal response in the TS is not

5 independent, but rather closely related to the tides in the ECS.

The southward and northward Kelvin waves obtained from Ex. 1 are shown in Figs. 5c and 5d respectively. Comparison of these figures with Figs. 4a and 4b indicates that in area A the southward wave is identical, but the northward wave from Ex. 1 is weaker. For the area x = 0 to 330 km, y = 0 to 200 km the area mean amplitude of the northward Kelvin wave is 0.57 m, which is smaller than the single area model value by 32%. In area B, the amplitudes of the transmitted southward Kelvin wave

10 are about 0.4 m, and those of northward wave are negligible. An important difference in co-phase-lag distributions is that Figs. 3a-c show a northward propagation along the south part of the eastern sidewall, while Fig. 5b does not have such a feature. This is because in single area case the amplitudes of the northward Kelvin wave are greater than those of the southward Kelvin wave in this area (Figs. 4a, 4b), while in Ex. 1 this situation does not occur (Figs. 5c, 5d).

The relative magnitudes of the incident, reflected and transmitted Kelvin waves can be evaluated by comparing their

15 amplitudes along the connecting cross section at $x = 400$ km. The sectional mean amplitudes for the incident, reflected and transmitted waves, H_i, H_r, and H_t, are 1.06, 0.63 and 0.40 m respectively (Figs. 5c, 5d). Thus the ratios H_r/H_i and H_t/H_i are equal to 0.60 and 0.38 respectively. The corresponding values based on the theory ignoring earth's rotation can be calculated from $\frac{H_r}{H_i} = \frac{1-\rho}{1+\rho}$ and $\frac{H_t}{H_i} = \frac{2\rho}{1+\rho}$ with $\rho = \sqrt{h_A/h_B}$ (e. g., Dean and Dalrymple, 1984, p. 144). Substitution of the present model depths into these equations yields $H_r/H_i = 0.63$ and $H_t/H_i = 0.37$. This indicates that the magnitude of the reflected waves

20 in two-dimensional case with the earth's rotation taken into account is smaller than that based on the theory with the earth's rotation ignored.
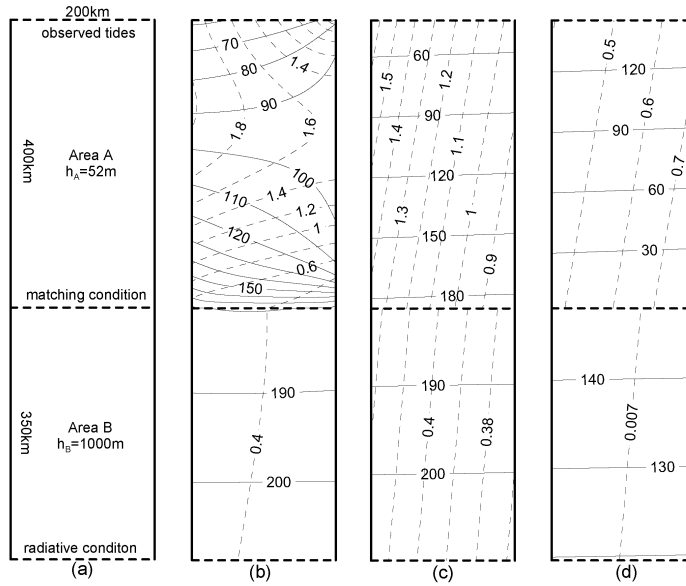
Figure 5. Model domain and boundary conditions of Ex. 1 (a); solution of Ex. 1 (b); southward Kelvin waves (c); northward Kelvin waves. Solid lines represent Greenwich phase-lag; dashed lines represent amplitude (in metres).

4.2 Influence of the shelf region southwest of the Taiwan Strait

5   From Fig.1 we can see that there is a narrow shelf along the mainland coast. To simulate the effect of the narrow shelf on the

tides in the TS we carry out the second experiment, numbered Ex. 2. In this experiment the deep basin is moved 60 km eastward,

allowing the tides in the shallow basin radiate freely southward as shown in Fig. 6a. The radiative condition (6) is retained

along the southernmost opening. The results of Ex. 2 are given in Fig. 6. It can be seen that the tides in area A have only small

changes though the deep basin is moved 60 km eastward. Observable changes can only be found in area B where the tidal

10   amplitudes are slightly reduced.
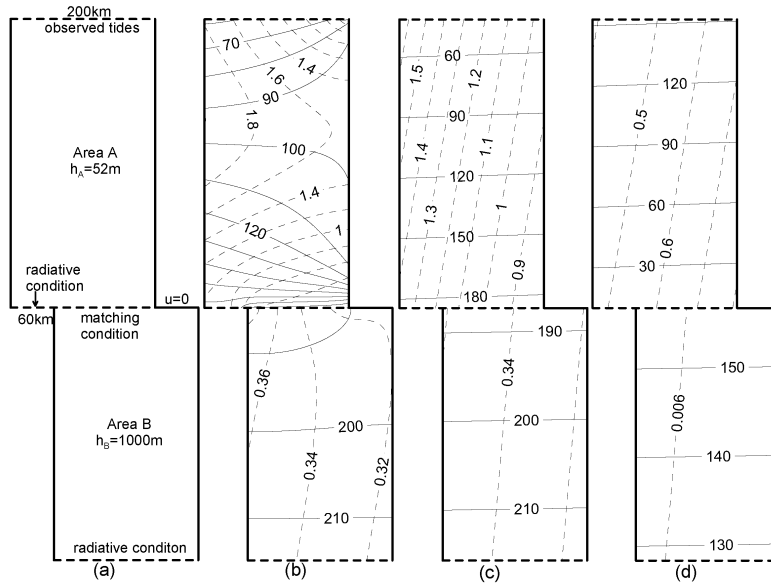
Figure 6. Same as Figure 5, but for Ex. 2.

4.3 Influence of the Luzon Strait forcing

The purpose of making the third experiment, numbered Ex.3, is to consider tidal input from the LS. The major difficultly in

5   including the LS input in the Taylor's model for the TS is that the LS has a meridional orientation, while the Taylor's model

does not allow to open any part of sidewalls. Here we will use a rather crude model to simulate this issue. We still use the same

model domain as Ex. 2, but the radiative boundary condition (6) is retained only for the west segment of the southernmost

opening, and the boundary condition (7) is applied to the remaining east segment of the opening. From Fig 1 we can see that

the cross section from the mainland shelf to the LS is much longer than the width of the LS, thus in our model we take the

10   lengths of the west and east segments to be 120 km and 80 km respectively as shown in Fig. 7a. In addition, from Fig. 2 we

observe that the tidal amplitude along the LS is roughly about 0.2 m, and the phase-lag is about 310 °. Since a significant part

of incident wave from the LS propagates toward the SCS deep basin (e. g., Fang et al., 1999; Yu. et al., 2015), we use a 0.1 m

amplitude and 310 ° phase-lag as an open boundary condition for the east segment of the southernmost opening in Ex. 3. The

model results are given in Figs. 7b to 7d. From Fig. 7b we can see that the amplitudes of the tide in area A now become greater

15   than the results of Ex. 2 (Fig. 6b), and a northward propagating character can be seen in the southeastern portion of area A.

These improvements can be attributed to the increased amplitudes of the northward Kelvin wave (Figs. 6d, 7d).
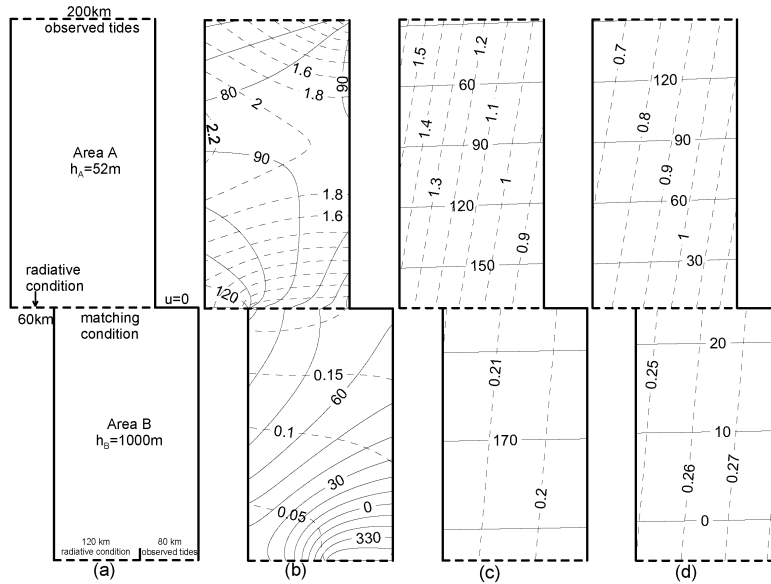
Figure 7. Same as Figure 5, but for Ex. 3.

5 Summary and discussion

In the present study we first establish an analytical model for M_2 tide in the TS using the extended Taylor' method. The

5 superiority of the analytical solution is that the tides can be decomposed into a southward Kelvin wave, a northward Kelvin

wave, and two families of Poincaré modes, providing a deeper insight into the dynamics of the tides in the area. Though the

coastlines and bottom topography are greatly simplified the model-produced pattern resembles the observed tidal regime

quite well. We then carry out several experiments to examine the formation mechanism of the northward propagating wave,

especially the roles of the abruptly deepened bottom topography south of the TS and the tidal forcing in the LS in the

10 formation of the northward wave. From this study we obtain the following results.

The M_2 tide in the TS can be basically represented the superposition of a southward propagating and a northward

propagating Kelvin waves, with the former stronger than the latter. The superposed Kelvin waves give an anti-nodal band

near the cross-strait transection roughly from Haitan Island to Taichung. The maximum amplitude on the mainland side is

greater than that on the Taiwan side, showing the cross-strait asymmetry. Therefore, the observed features can be reproduced

15 by the composition of a stronger southward propagating and a weaker northward propagating Kelvin wave. In this regard,

the Coriolis force and friction play essential roles.

Inclusion of the Poincaré modes into the analytical model can improve the model result: the east to west increase in

amplitudes along the northern and southern openings can be better reproduced; and in particular, the Poincaré modes have

approximately the same contribution as the Kelvin waves to the cross-strait asymmetry in the anti-nodal band.

The reflection of the southward wave at the abruptly deepened topography south of the TS is a major contribution to the formation of the northward propagating wave in the strait, though the reflected wave is slightly weaker than that obtained from the analytical solution with open boundary conditions determined by observations. Inclusion of the tidal forcing at the LS can strengthen the northward Kelvin wave in the TS, and thus improves the model result. This indicates that the LS

5 forcing is of some (but lesser) importance to the TS tides.

The analytical solutions can help us to understand the dynamics of tidal motion in the TS, but there are some limitations. For example, the LS is located on the east side of the study area, while Taylor's model does not allow a forcing on the sidewalls, thus we are bound to let a part of southern opening represent the LS (Fig. 7a). In addition, we have assumed that the water depths change from 52 m to 1000 m immediately at the connecting cross section without considering the existence of

10 continental slope there. The obliqueness of the orientation of the topography step relative to the cross-strait direction is also ignored. These approximations will induce uncertainty in the result for the magnitude of reflected wave.

Acknowledgements. This study was supported by the NSFC-Shandong Joint Fund for Marine Science Research Centers (Grant No. U1406404), the Basic Scientific Fund for National Public Research Institutes of China (Grant No. 2014G15), and

15 the National Key Research and Development Program of China (Grant No. 2017YFC1404201).

References

Cheng, Y. C., and Andersen, O. B.: Multimission empirical ocean tide modeling for shallow waters and polar seas, Journal of Geophysical Research: Oceans, 116, 1130-1146, 2011.

Cui, X., Fang, G., Teng, F., and Wu, D.: Estimating peak response frequencies in a tidal band in the seas adjacent to China

20 with a numerical model, Acta Oceanologica Sinica, 34, 29-37, 2015.

Dean, R. G. and Dalrymple, R. A.: Water Wave Mechanics for Engineers and Scientists, World Scientific Publishing Co. Pte. Ltd, Singapore, 353 pp., 1984.

Defant, A.: Physical oceanography, Vol. II, Pergamon Press, New York, 598 pp, 1961.

Fang, G. H. and Wang, J. S.: Tides and tidal streams in gulfs, Oceanologia et Limnologia Sinica (in Chinese with English

25 abstract), 1966.

Fang, G. H., Yang, J. F., and Thao, Y. C.: A two-dimensional numerical model for tidal motion in the Taiwan Strait, Marine Geophysical Research, 7, 267-276, 1984.

Fang, G. H., Kwok, Y. K., Yu, K. J., and Zhu, Y. H.: Numerical simulation of principal tidal constituents in the South China Sea, Gulf of Tonkin and Gulf of Thailand, Continental Shelf Research, 19, 845–869, 1999.

Fang, Z., Ye, A. L., and Fang, G. H.: Solutions of tidal motions in a semi-closed rectangular gulf with open boundary condition specified, Tidal Hydrodynamics, edited by: Bruce, P. B., John Wiley & Sons. Ins., New York, 153-168 pp., 1991.

Godin, G.: Some remarks on the tidal motion in a narrow rectangular sea of constant depth, Deep-Sea Research, 12, 461-468, 1965.

Hu, C. K., Chiu, C. T., Chen, S. H., Kuo, J. Y., Jan, S., and Tseng, Y. H.: Numerical simulation of barotropic tides around Taiwan, Terrestrial Atmospheric & Oceanic Sciences, 212502, 71-84, 2010.

Jan, S., Chern, C. S., and Wang, J.: Transition of tidal waves from the East to South China Seas over the Taiwan Strait: Influence of the abrupt step in the topography, Journal of Oceanography, 58, 837-850, 2002.

Jan, S., Chern, C. S., Wang, J. and Chao S. Y.: The anomalous amplification of M_2 tide in the Taiwan Strait, Geophysical Research Letters, 31, L07308, doi:10.1029/2003GL019373, 2004a.

Jan, S., Wang, Y. H., Wang D. P., and Chao, S. Y.: Incremental inference of boundary forcing for a three-dimensional tidal model: tides in the Taiwan Strait, Continental Shelf Research, 24, 337-351, 2004b.

Jung, K. T., Park, C. W., Oh, I. S., and So, J. K.: An analytical model with three sub-regions for M_2 tide in the Yellow Sea and the East China Sea, Ocean Science Journal, 40, 191-200, 2005.

Lin, M. C., Juang, W. J., and Tsay, T. K.: Application of the mild-slope equation to tidal computations in the Taiwan Strait, Journal of Oceanography, 56, 625-642, 2000.

Lin, M. C., Juang, W. J., and Tsay, T. K.: Anomalous amplifications of semidiurnal tides along the western coast of Taiwan, Ocean Engineering, 28, 1171-1198, 2001.

Lü, X. G. and Sha, W. Y.: Three-dimensional numerical simulation of M_2 tide in the Taiwan Strait. Journal of Oceanography of the Huanghai and Bohai Seas, 17, 16-25 (in Chinese with English abstract), 1999.

Rienecker, M. M. and Teubner, M. D.: A note on frictional effects in Taylor's problem. Journal of Marine Research, 38, 183–191, 1980.

Roos, P. C. and Velema, J. J.: An idealized model of tidal dynamics in the North Sea: Resonance properties and response to large-scale changes. Ocean Dynamics, 61, 2019-2035, 2011.

Taylor, G. I.: Tidal oscillations in gulfs and rectangular basins. Proceedings of the London Mathematical Society, Ser. 2, 20, 148–181, 1922.

Ye, A. L., Chen, Z. Y., and Yu, Y. F.: Numerical investigation of three-dimensional semidiurnal waves in the Taiwan Strait and its adjacent areas, Oceanologia et Limnologia Sinica, 16, 439-450, 1985 (in Chinese with English abstract).

Yin, F., and Chen, S. H.: Tidal Computation on Taiwan Strait, Journal of the Waterway Port Coastal & Ocean Division, 108, 539-553, 1982.

Yu, H. Q., Yu, H. M., Ding, Y., Wang, L., Kuang, L.: On M_2 tidal amplitude enhancement in the Taiwan Strait and its asymmetry in the cross-strait direction, Continental Shelf Research, 109, 198-209, 2015.

Yu, H. Q., Yu, H. M., Wang, L., and Kuang, L., Wang, H., Ding, Y., Ito, S. I., and Lawen, J.: Tidal propagation and dissipation in the Taiwan Strait, Continental Shelf Research, 136, 57-73, 2017.

5   Zeng, G., Hu, J., Hong, H., and Qi, Y.: Numerical study on M_2 tidal system in the Taiwan Strait, Procedia Environmental Sciences, 12, 702-707, 2012.

Zhu, J., Hu J. Y., Zhang, W. Z., Zeng, G. N., Chen, D. W., Chen J. Q., Shang S. P.: Numerical study on tides in the Taiwan Strait and its adjacent area, Marine Science Bulletin, 11(2), 23-36, 2009.